A Time-domain Reflectometry Method for Automated Measurement of Crack Propagation in Composites during Mode I DCB Testing

A. Abu Obaid,[1,*] S. Yarlagadda,[1] M. K. Yoon,[1]
N. E. Hager III[2,3] and R. C. Domszy[2]

[1]*Center for Composite Materials, University of Delaware, Newark, DE 19716, USA*
[2]*Material Sensing and Instrumentation, Inc. Lancaster, PA 17601-2212, USA*
[3]*Department of Physics and Engineering, Elizabethtown College, Elizabethtown PA 17022, USA*

(Received September 5, 2005)
(Accepted October 10, 2005)

ABSTRACT: This article describes a new technique for automated measurement of crack initiation, growth, and propagation in composite materials during mode I double cantilever beam (DCB) testing. The proposed method uses time-domain reflectometry (TDR) to detect changes in geometry and electromagnetic properties (dielectric or magnetic) along a transmission line that can be embedded in or bonded to the surface of the specimen. Two types of transmission line TDR sensors are evaluated (IM7 carbon fiber and ARACON) during DCB tests. A P-SPICE transmission-line simulation model is used to verify the baseline signal response for the DCB sensor and the sensitivity for crack detection, with good agreement. Comparison with standard visual methods in DCB testing showed excellent correlation in crack location, crack propagation (L_C), and the interlaminar fracture toughness (G_{IC}) values. The TDR sensor design and model-based parametric studies are carried out to determine optimal sensor geometry and configuration. The results demonstrate that the TDR-based method can measure crack propagation parameters at high resolution and accuracy, in an automated manner using low-cost sensors.

KEY WORDS: composite materials, DCB testing, TDR sensors, crack propagation, fracture toughness.

*Author to whom correspondence should be addressed. E-mail: abuobaid@ccm.udel.edu
Figure 5 appears in color online: http://jcm.sagepub.com

0021-9983/06/22 2047–20 $10.00/0 DOI: 10.1177/0021998306061309

INTRODUCTION

Fracture toughness is an important parameter in the mechanical performance of composite materials, as it relates to the ability of the material to resist crack initiation and propagation. Crack initiation and propagation in composites typically occurs due to interlaminar stress concentrations whether it is due to a free edge, ply drops, joints, or notches. Crack growth in composite materials is classified into three modes: mode 1 (the crack faces are pulled apart), mode 2 (the crack surfaces slide over each other), and mode 3 (the crack surfaces move parallel to the leading edge of the crack and relative to each other). A standardized method for measuring fracture toughness of composite materials in mode 1 is the double cantilever beam (DCB) method, as described in ASTM 5528 [1].

In the DCB test method (Figure 1), the ends of the specimen are pulled apart forcing a crack to propagate down the length of the beam. The progress of the crack is monitored as a function of the load and cross-head displacement, and used to calculate the strain energy release rate (or called as interlaminar fracture toughness of the material).

There are several methods currently in use to monitor the progress of the crack during the test. The most common method is a visual technique using a monoscope or a traveling microscope of low magnification. This method requires marking the side of the test specimen and monitoring the crack progression by arrival at each mark. It is a time-consuming method that has limited resolution (± 0.5 mm) and somewhat subjective in nature. Low toughness materials may also pose a problem, due to rapid crack initiation and propagation. Several techniques have been developed to automate the process, especially in polymers and are primarily optical or electrical-based methods.

Uhlig et al. [2,3] developed an automated optical crack tracing system that uses a CCD camera to monitor the crack front during the test, with real-time image processing to obtain crack propagation data. A fully automated system is available [3] that requires no additional sample preparation time, has a high degree of accuracy, and can complete the test rapidly. However, this method requires a direct view of the tested specimen, which may not be possible under extreme environmental conditions (hot-wet, low temperature, etc.).

Crack gages are available from several sources, and though they have different configurations, they essentially rely on change in electrical properties of a surface bonded system, as the crack propagates through it. One version uses a foil configuration [4], which

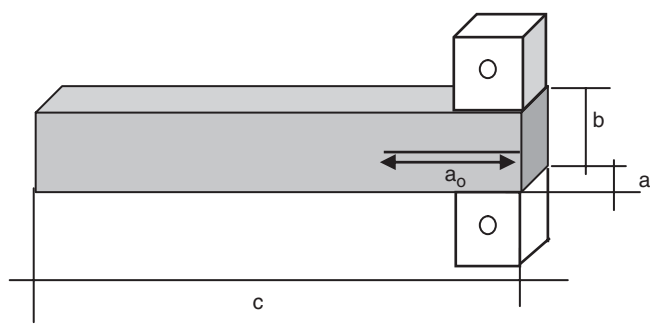

Figure 1. *Typical DCB-specimen configuration for mode 1 fracture toughness, where the dimensions a, b, c, and a_0 are specimen width, specimen thickness, specimen length, and initial delamination, respectively.*

cracks during the test, and a second version [5] uses an array of conductive wires that break in sequence as the crack front moves through the gage. Crack gages are mounted on the side face of the DCB test specimen and can get expensive for longer beam type coupons. The foil-based gage requires substantial thickness for mounting (> 0.5 in.), while the conductive wire array gage is limited in resolution and cost. Both gage methods require substantial specimen preparation prior to testing. None of these methods have the combination of low cost, non-intrusive or *in-situ*, usability under extreme conditions, and simplified specimen preparation, at the same time.

In this article, we demonstrate a time-domain reflectometry (TDR) based technique as a novel automated sensing method for crack propagation measurement that meets all these requirements. The sensors are essentially high frequency transmission lines, with the signal and ground signal paths straddling the crack plane and can be integrated into the composite specimen during manufacture or surface bonded. In addition, any conductive material (metal wires, carbon fibers, metal-clad fibers, etc.) is a potential sensor material, with little performance degradation. The system can be fully automated, has higher resolution than current crack sensors and can perform in extreme environments (hot and humid conditions), as no visual tracking is necessary.

BACKGROUND

Time-domain reflectometry (TDR) is a method of sending a fast pulse down a controlled-impedance transmission line and detecting reflections returning from impedance discontinuities along the line. The basic configuration is shown in Figure 2, where the TDR oscilloscope is shown on the left which both supplies the input voltage step and captures the returning signal. The extension from the oscilloscope is a controlled-impedance transmission line (typically a co-axial conductor), which is embedded within the material and is used as a linear sensing element. Any change in dielectric or magnetic properties and geometry in the vicinity of the transmission line, causes a reflection (impedance discontinuity) which can be located by propagation delay. Time scales are fast, of the order 10–100 ps/cm (GHz frequencies), so reflections occurring at different positions in the line are separated by propagation delay, forming a 'closed-circuit radar'. As the equivalent frequencies are in the communications range, the TDR method is commonly used in locating faults in networking and cable-TV systems.

The TDR has gained popularity in recent years as a diagnostic tool in infrastructure applications by evaluating changes in dielectric properties or geometry [6]. The transmission line is embedded in a bridge or highway structure, such that a flaw in the surrounding structure causes a mechanical distortion in the line. Similar methods are used

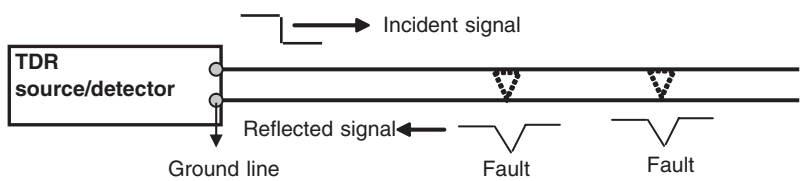

Figure 2. *Basic TDR fault detection.*

in groundwater level detection, where the line is embedded in a soil layer such that the groundwater level causes a permittivity change.

The TDRs can be applied to smaller-scale applications such as composite parts provided the propagating pulse is sufficiently localized. Typical infrastructure applications use pulse widths around 500 ps with input bandwidths near 2 GHz, producing an effective size resolution around 100 mm. This resolution is sufficient for infrastructure applications, but for composite parts is an order of magnitude too high. Composite parts require pulse localization below 10 mm, and such instrumentation with pulse widths around 35 ps and input bandwidths near 20 GHz is now becoming available.

The TDR sensors have been developed for other composite material applications including resin flow monitoring [7], composite cure monitoring [8,9], and structural health monitoring [10]. The system has been proven to accurately measure distributed parameters such as resin flow position, degree of cure, defect position, and strain. The transmission line is embedded either in the part or on its surface, or it can be integrated into the tooling making it reusable as well as sensing through gel coats commonly applied to mold surfaces. The TDR sensors are unique in that they are lineal sensors which can interrogate distributed changes along their entire length, rather than at discrete points as with fiber optic sensors. This reduces the number of sensor lines and associated acquisition hardware.

TDR Sensor for Crack Detection in DCB

The sensor geometry used for crack propagation detection consists of a signal path and ground plane straddling the crack plane in simple transmission line configuration [11] (Figure 3). The transmission impedance is calculated from the geometry using various shareware transmission-line calculators [12]. The target impedance is 50 Ω, though higher impedances can be useful for reduced attenuation. The ends of the signal and ground lines are crimped with a small copper ring and a SMA type connector is soldered to connect to the TDR source (Figure 3).

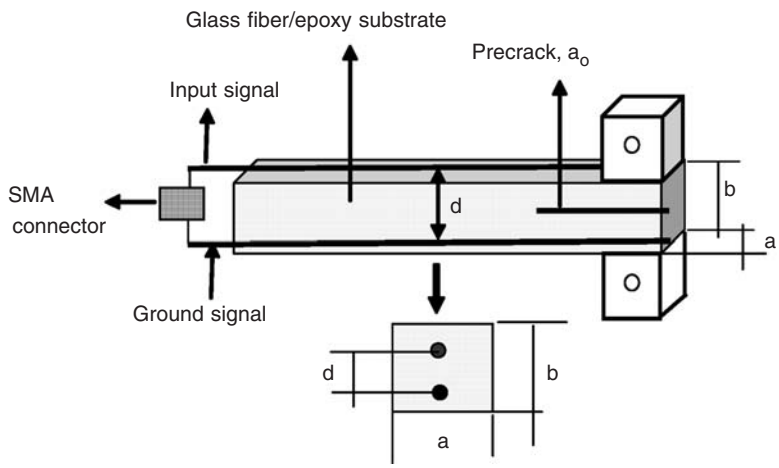

Figure 3. *TDR-sensor configuration for mode 1 DCB test, where d is the distance between the signal line and the ground line.*

In our previous work [13], it has been shown that TDR sensors are good crack detection and propagation sensors for the mode 1 DCB configuration. The sensor showed excellent correlation with the standard visual method when comparing the crack location during the test and provided significantly higher resolution. This effort represents a continuation of the previous work and documents data reduction methodologies, fracture toughness comparisons, and model-based parametric studies for optimal sensor configuration.

EXPERIMENTAL SETUP FOR TDR CRACK SENSOR

DCB Sample Preparation

Double cantilever beam (DCB) specimens were fabricated to evaluate the ability of TDR sensors to automate crack-growth measurement, as shown in Table 1. The panels were fabricated by infusing SC79 epoxy into 8 layers of S2 glass fabric (area density of 24 oz/yd^2) using the vacuum-assisted resin transfer molding (VARTM) process. The panels were cured at room temperature for 36 h and post-cured at 250°F for 4 h, and then cut into coupons 25 mm wide and 300 mm long. An initial delamination was made by inserting a 50 μm thick Kapton film at the mid-plane of the laminate. Two types of sensor materials were evaluated (Table 1) and are described in the following section. The initial delamination or insert length was 55 mm for specimens of type 1, and 50 mm for specimens of type 2.

Aluminum cubes (25×25 mm) were bonded to each side of the DCB specimen where the initial delamination was made, using an overnight room-temperature adhesive. One specimen each of types 1 and 2 was used to compare TDR with visual or optical techniques and the edge of the specimens were painted white with enamel and marked at 1 mm intervals for visual monitoring of the crack length. Remaining specimens were evaluated in 'blind' tests of the TDR configuration.

TDR Sensor Description

Two sensor types were evaluated to demonstrate flexibility in the sensor material, the first using two carbon fiber thermoplastic prepreg tapes (3 mm wide IM7/PEI) and the second using ARACON fiber tows (conductive KEVLAR tow consisting of 67 monofilaments) as both the signal and ground in the transmission line. While the

Table 1. Specifications of the DCB test specimens.

Sample type	DCB type	Substrate	Sensor/ground	Sensor length (mm)	Sensor resistance per unit length (Ω/m)
1	Resin DCB SC79 epoxy	S2-glass woven fabric/SC 79 epoxy	ARACON fiber tow	300	1.3
2	Resin DCB SC79 epoxy	S2-glass woven fabric/SC79 epoxy	Carbon fiber thermoplastic prepreg tape (IM7/PEI)	211	50

transmission line configuration only requires a conductor, and the structural conductive fibers were selected to match materials in the substrate. For all DCB coupons, the signal line and the ground line were placed (embedded during substrate fabrication) axially down the center of each coupon, straddling the expected crack plane. The parallel distance (d) between the signal line and ground line was 6 mm for all specimens (Figure 3).

TDR Equipment Setup

The equipment used for recording data was an Agilent Technologies HP54750 digitizing oscilloscope with a 54754A differential TDR plug-in. The scope has a 10 ps/cm maximum sweep speed and 18 GHz input bandwidth, with a 35 ps risetime step applied internally across the input. Each TDR signal has a maximum resolution of 4096 points, which essentially resolves the length of the TDR sensor line into 4096 intervals. The acquisition rate is approximately one signal or sweep per second and is as a function of hardware capability, and higher rates can be achieved using a PC-based system or improved data handling from the scope. To reduce noise signal, averaging is performed over 16 individual sweeps, yielding an averaged sweep with improved signal resolution. The averaging reduces the number of total data points (crack locations) approximately to 2–300 per DCB test (one every 16 s).

Test Method and Data Acquisition

The specimens were mounted in a fixture to load the end blocks (Instron 4484 static load frame) and the end of the specimens was supported in order to keep the beam orthogonal to the direction of the applied load. All tests were performed at crosshead speed of 1.3 mm/min and a 100 lb load cell was used. For all tests, the TDR data acquisition system and the test frame (Instron machine) were synchronized, so that the correlation of the TDR response (signal time shift) to the crack event occurring in the specimens was accurate.

DATA REDUCTION METHODOLOGY

Crack Front Movement

Figure 4 is a representative TDR signal sequence measured during DCB test, regardless of the sensor type or specimen type. For all cases, the baseline (reference signal when the load is zero) shows the usual signal injection on the left and open-circuit reflection on the right (Figure 4). As loading begins, the crack propagates causing the signal-ground spacing and consequently impedance to increase at the loaded end of the coupon causing the signal rise from the initial baseline. The position along the time axis (correlates to location based on propagation velocity in the sensor) at which this initial rise occurs is the crack front which moves to the left, as the crack propagates in the specimen.

The crack length, L_C, is determined from TDR signal as shown in Figure 5. Injection of the TDR pulse at the sensor input (beginning of TDR sensor) is shown at position t_1 while a reflection of the pulse from far-end termination (end of TDR sensor) is shown

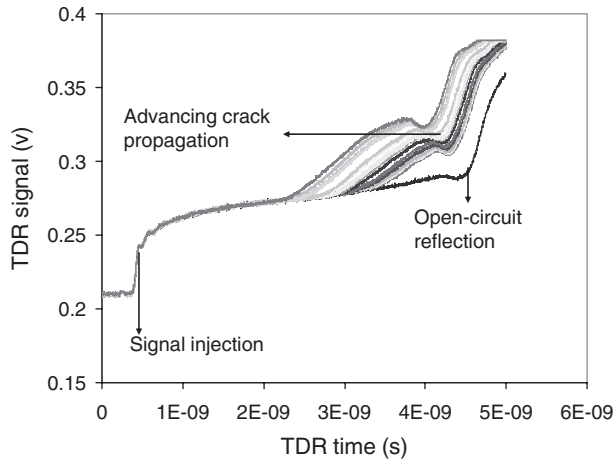

Figure 4. *Representative DCB signal evolution for TDR crack sensor.*

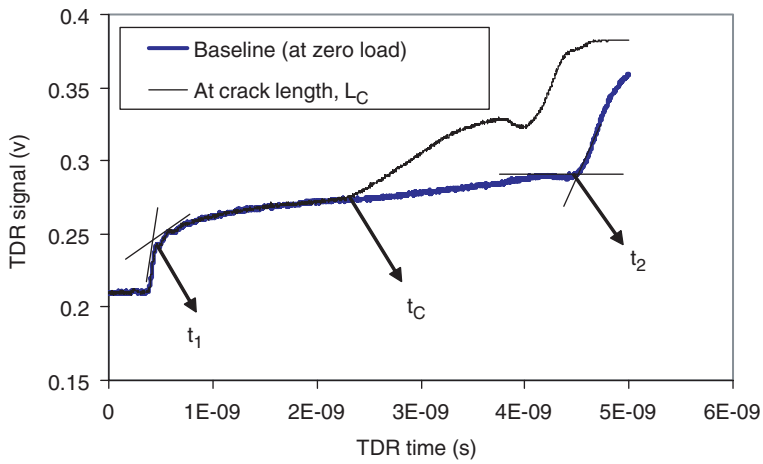

Figure 5. *Timing markers in the TDR crack sensor signal that are used to determine crack length during a DCB test.*

at position t_2. The location of the crack as determined by the position at which the signal departs from the initial baseline as shown at position t_C. The crack length is determined by the timing shift $(t_2 - t_C)$ between the far-end reflection t_2 and the crack position t_C. The total horizontal opening L_{opening} is the horizontal distance from the end of the specimen to the crack tip t_C as measured in the direction of the crack at the mid plane of the specimen. The horizontal opening L_{opening} is thus calculated as

$$L_{\text{opening}} = \frac{v(t_2 - t_C)}{2} \tag{1}$$

where v is the propagation velocity in the sensor of length L_0 as calculated by

$$v = \frac{2L_0}{t_2 - t_1} \tag{2}$$

Combining Equations (1) and (2) gives the crack opening L_{opening} as

$$L_{\text{opening}} = \frac{L_0(t_2 - t_C)}{t_2 - t_1} \tag{3}$$

Since the total crack opening includes the crack length L_C and the initial delamination a_0 (length of the Kapton insert), the actual crack length L_C is thus given as

$$L_C = L_{\text{opening}} - a_0 \tag{4}$$

The TDR time markers t_1 and t_2 are determined by the intersections of lines obtained from extrapolation of the sections of maximum slope [14]. The location of timer marker t_C is based on the deviation of the TDR signal from the baseline. Due to noise present in the signal, a statistical threshold limit (α) is used to obtain the deviation from the baseline. This threshold value is calculated as

$$\alpha = A\sigma\{t_1, t_2\} \tag{5}$$

where σ represents the average standard deviation of the difference between the signal and the baseline, obtained between times t_1 and t_2, A is a constant that depends on the degree of noise in the signal and allows elimination of outliers. As shown in Figure 6, the noise in the results of the total crack length is significantly higher when $A < 3$ with a value of 3.5 essentially eliminating all noise. A value of 3.5 was selected for all data reduction in this study. In a physical sense, a higher value of A requires a higher deviation of the signal from the baseline.

For automated data reduction during the experiment, a special software routine (LabView program) was developed. The operational steps of the program are presented as a flowchart in Figure 7. First, the program reads the TDR baseline data set $\{B_i(t)\}$

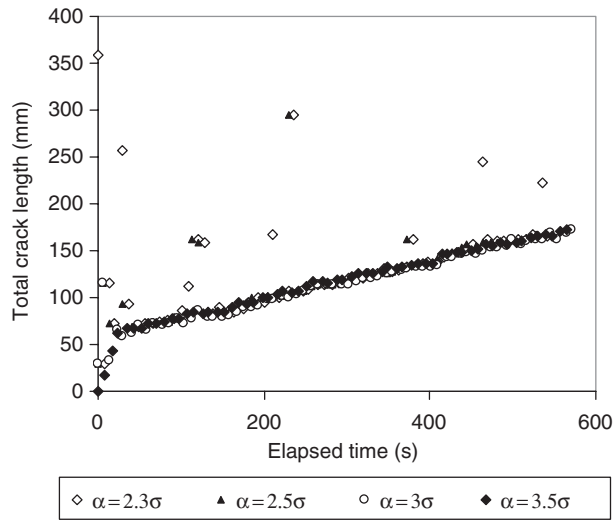

Figure 6. *Total crack length calculated for different values of the constant (A). A value of 3.5 is selected for all subsequent calculations.*

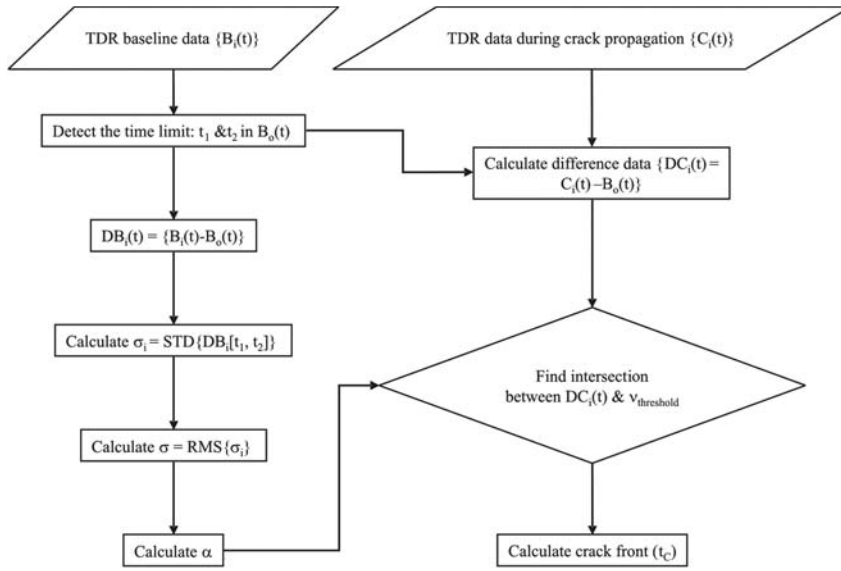

Figure 7. *Flowchart showing the steps for automated calculation of the crack front location. The rank i is the number of the TDR record or dataset.*

obtained before the crack propagation. σ is obtained from the root mean square of the standard deviation of the baseline difference data set $\{DB_i(t)\}$ between the time interval t_1 and t_2. Then, the threshold level obtained from Equation (5) is compared with the TDR difference data set $\{DC_i(t)\}$ in order to detect the TDR signal delay time t_C, which correlates to the crack location at each time step.

Fracture Toughness Calculation

The interlaminar fracture toughness G_{IC} is determined by applying the compliance calibration (CC method) according to ASTM D5528, which is given by:

$$G_{IC} = \frac{n * \delta * P}{2 * a * L_{CT}} \tag{6}$$

where L_{CT} is the total crack length ($L_{CT} = L_C + a_0$), P the applied load, δ the load point displacement, and a the specimen width. The term n is the slope of the plot log J–log(L_{CT}), where J is the compliance which is equal to δ/P. The load–displacement information is obtained directly from the Instron mechanical tester while the crack propagation length is measured either by traveling microscope or from the time shift of the TDR signal.

EXPERIMENTAL RESULTS

Initial measurements were conducted using the ARACON-based TDR sensor (type 1). For the three DCB specimens tested, the obtained L_C values using TDR-method were

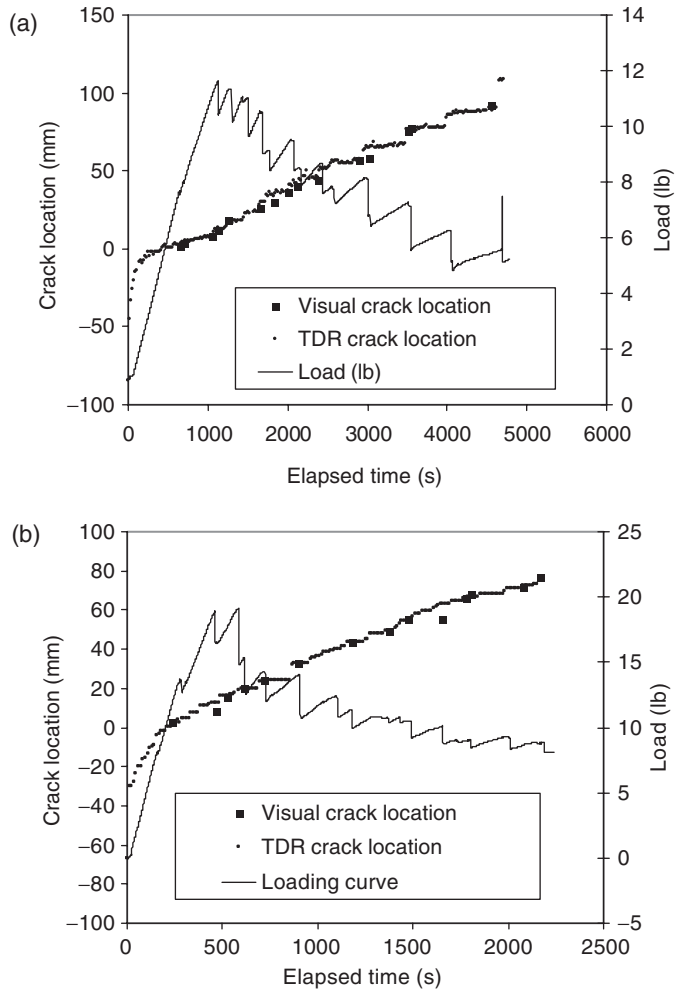

Figure 8. *(a) Comparison of TDR sensor and visual crack length for DCB specimen (type 1, ARACON fiber tow sensor) and (b) comparison of TDR sensor and visual crack length for DCB specimen (type 2, IM7/PEI sensor).*

compared with the values measured visually using the traveling microscope. The developed Labview program was applied to each TDR sequence to measure the time delay t_C as a function of the elapsed time applying threshold values, as discussed earlier. From the obtained time delay t_C, the L_C values were calculated applying Equations (3) and (4). Figure 8(a) and (b) show the representative behavior of L_C and the load as a function of elapsed time for both specimen types.

For both types of specimens the crack propagation occurs when $L_C > 0$, whereas there is no crack propagation occurring when $L_C < 0$ and therefore, the negative values of the L_C are obtained according to Equation (4). Furthermore, when $L_C = 0$, the total opening in the specimens equals to the length of the initial insert delamination (i.e., $L_{opening} = a_0$). Figure 8(a) and (b) also show a representative comparison of the crack location data between the TDR sensor and the traveling microscope based method. As

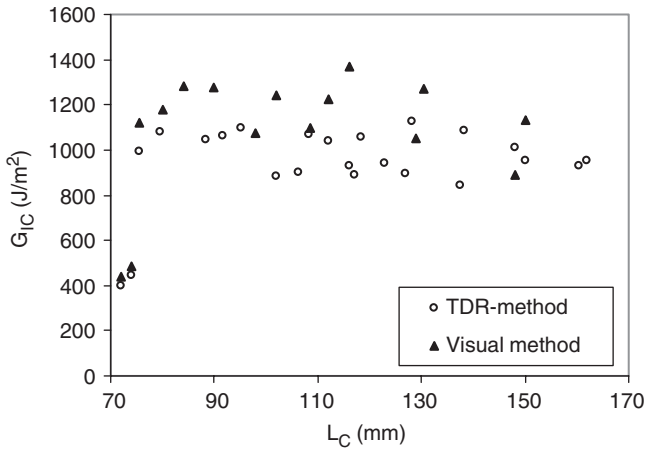

Figure 9. *Comparison of G_{IC} between TDR sensor and visual method for DCB specimen (type 1).*

expected, the results indicate that the TDR sensor provides much higher resolution in terms of crack location, compared to visual techniques, while providing an automated method to measure crack location. The enhanced resolution allows more accurate determination of the crack location as a function of the selected loading points. Similar conclusions were obtained for DCB adhesive specimens tested in our previous work [13].

From the behavior of the TDR signal response to the load as shown in Figure 8(a) and (b), an interesting feature to note is that the TDR method has enough resolution to track the stick–slip behavior that is the characteristic of fiber-reinforced composites. Further refinements in both the data acquisition strategy, averaging and sensor optimization can lead to more accurate measurements for tracking stick–slip behavior.

Fracture Toughness

Using the crack length values in combination with their corresponding critical load and displacement values, the interlaminar fracture toughness G_{IC} values were determined based on Equation (6). A comparison of the calculated fracture toughness values based on the crack locations in Figure 8 are shown in Figure 9. The TDR method is able to generate a higher number of data points (23 compared to 15) due to the more accurate tracking of crack length as a function of the loading curve.

A comparison of the interlaminar fracture toughness G_{IC} for both sets of specimens is shown in Table 2. The initiation G_{ICO} and propagation G_{ICP} values compare extremely well for both types of sensors, proving the robustness of the technique and its independence on the sensor material.

In summary, experiments have shown automation, improved resolution and accuracy of the proposed TDR crack sensor compared to the standard visual techniques, for fiber-reinforced composites. The sensor is integrated into the specimens during manufacture and is extremely low-cost. However, the influence of the sensor parameters on the sensor performance is not clear, specifically, signal–ground plane spacing

Table 2. Fracture toughness values for TDR sensor.

Sample type	Substrate	Sensor	G_{ICO}	G_{ICP}
1	S2- glass woven fabric/SC 79 epoxy	ARACON fiber tow	517 ± 119	1000 ± 85
2	S2- glass woven fabric/SC79 epoxy	Carbon fiber thermoplastic Prepreg tape (IM7/PEI)	483 ± 119	882 ± 109

(6 mm was used in this work), sensor material resistance, signal and ground plane relative planar dimensions. The effect of these parameters on the TDR signal response will be discussed in the following sections.

MODEL-BASED PARAMETRIC STUDIES FOR TDR CRACK SENSOR

The influence of crack sensor parameters (such as substrate type and sensor geometry on the TDR signal response) was evaluated using a P-SPICE transmission line model [15]. The model was developed to verify both the baseline signal response for the TDR DCB crack sensor as well as for sensitivity and parametric studies. The P-SPICE is a commercially available circuit simulation program that is used to generate an equivalent circuit model for the TDR sensor. The transmission impedance and propagation velocity are obtained from the measured baseline voltage and propagation delay in the TDR sensor, and used to determine appropriate values for capacitance and inductance per unit length of the sensor (used in P-SPICE simulation). From transmission line theory [16], the impedance Z and velocity v are related to the capacitance and inductance according to:

$$Z = \sqrt{\frac{L}{C}} \tag{7}$$

$$v = \frac{1}{\sqrt{LC}} \tag{8}$$

Providing a unique value for L and C for the measured impedance and propagation velocity.

A P-SPICE model which matches the impedance and propagation velocity for a 300 mm long DCB sensor (IM7/PEI) is shown in Figure 10. On the left is the TDR signal source, which simulates a current pulse with a 35 ps rise time across a 50 Ω impedance. Immediately to the right is a lossless transmission section with 50 Ω impedance which simulates the sampling head of the oscilloscope. Further to the right is a lossy transmission section with adjustable capacitance, inductance, and resistance per unit length which simulates the DCB sensor or transmission line. The lossy transmission line section terminates in a capacitor C which represents the fringing capacitance of the open sensor termination end and a resistor R prevents a floating DC for the purpose of P-SPICE simulation.

The parameters used in the simulation are shown in Figure 10. A 0.485 μH/m inductance and a 95.5 pF/m capacitance provides a 71 Ω impedance to match the vertical baseline as

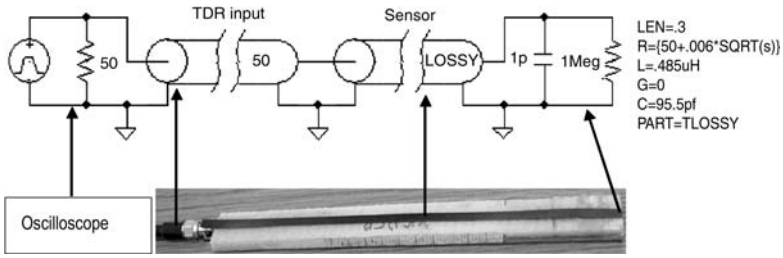

Figure 10. *P-Spice simulation of DCB sensor. The figure features the circuit elements and their corresponding components on DCB specimen.*

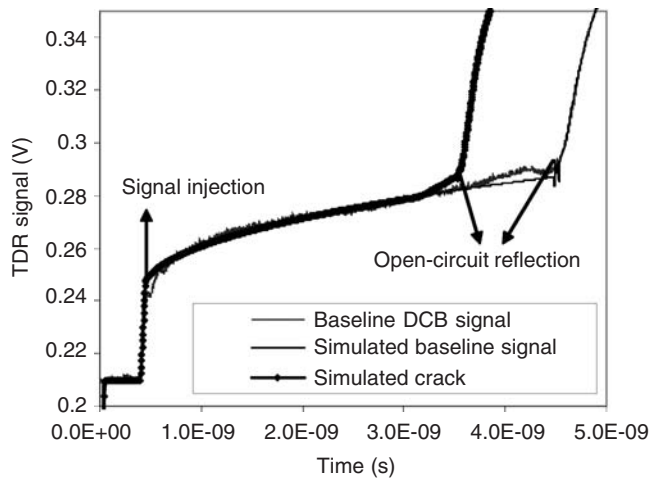

Figure 11. *P-SPICE simulation compared to experimental data for the baseline signal and the presence of the crack plane.*

well as a 1.47×10^8 m/s propagation velocity to match the round-trip propagation time. In addition, a 50 Ω/m resistive loss simulates the finite conductivity of the sensor material (measured for IM7/PEI tape), matching the rising slope of the propagating baseline. Finally, a $0.006\sqrt{f}$ skin-depth term represents the limited field penetration of the conducting material at high frequencies (f), which results in a preferential attenuation of the high-frequency components [16]. The skin-depth term matches the rounding of the reflected signal.

A comparison of the P-SPICE simulation with the baseline signal is shown in Figure 11. The pulse enters the sensor on the left and shows the expected increase in propagation impedance going from the 50 Ω sampling head to the 71 Ω DCB sensor. The baseline slopes upward with resistive loss in the sensor during propagation and shows the open-circuit reflection from the high-impedance far end (end of sensor line). The open-circuit reflection shows the expected rounding due to high-frequency attenuation, and small differences between simulation and experiment can be attributed to iteration errors.

The model can also be used to estimate the effect of crack propagation in the DCB sensor. The crack opening causes an increase in spacing between signal and ground paths

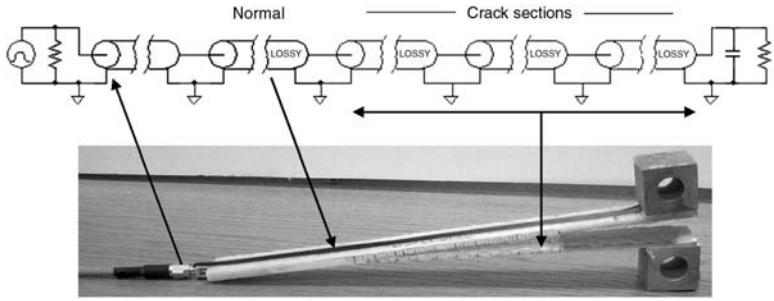

Figure 12. *P-SPICE simulation of sensor including crack section. The figure shows the circuit elements and their corresponding components on DCB specimen.*

and can be simulated by decreasing the capacitance and increasing the inductance per unit length in the model. Figure 12 shows a P-SPICE simulation which adds a crack section to the DCB model. Starting with the baseline configuration in Figure 10, the capacitance is then decreased linearly at 1 pf/mm with the inductance increased at 0.006 μH/mm to simulate the presence of a crack. The line is again terminated with the open-circuit reflection, and the result superimposed on the baseline sensor signal (Figure 11).

The simulated crack response is shown in Figure 11, where the DCB line with added crack section is superimposed on the original uncracked line. The original uncracked line is shortened to indicate the advancing crack location, with the open-circuit reflection appearing at an earlier time in the figure. The crack is simulated by three 5 mm long sections, where each section represents a 5% decrease in line capacitance between signal and ground paths, corresponding to a 5% increase in spacing. For the 6 mm strip spacing in Figure 3, this constitutes a sensitivity of the order of 0.3 mm, indicating that the signal is being detected near the leading edge of the crack formation.

TDR Crack Sensor Parametric Studies

Parametric studies were conducted using the P-SPICE transmission line model to evaluate the effect of the various parameters on sensor performance. The parameters considered in this study are conductivity of the substrate, conductivity of the sensor (sensor type), sensor geometry (radius (r) and width (w) of the sensor), and distance between the signal line and ground line (d) (see Table 3 and Figure 13).

DCB Substrate Conductivity

Initial evaluations of the TDR sensor were performed on dielectric substrates (glass/epoxy). Of particular interest is the effect of a substrate material that has varying degrees of electrical conductivity, as a conductive substrate can act as an electrical short between the signal and the ground lines of the transmission line configuration, thus rendering the sensor unusable. This is of particular interest when the substrate material is either a carbon fiber composite or a metallic material.

Table 3. Parametric study inputs for TDR sensor.

Sensor type	Parameter	Substrate	*d*	Dimensions
IM7/PEI tape	Sensor type**	Glass fiber/epoxy*	6 mm	$w = 4$ mm
ARACON tow	Sensor type**	Glass fiber/epoxy*	6 mm	$r = 1.52$ mm
Copper wire	Sensor type**	Glass fiber/epoxy*	6 mm	$r = 1.52$ mm
Copper wire	Sensor geometry	Glass fiber/epoxy*	6 mm	r varies from 0.1255 to 1.52 mm
ARACON tow	Sensor geometry	Glass fiber/epoxy*	It varies from 4 to 16 mm	$r = 1.52$ mm
IM7/PEI tape	Substrate conductivity	A substrate with G varying from 0 to 50	6 mm	$w = 4$ mm

*: This substrate material has G value (conductivity per unit length) of zero.
**: Sensor type refers to the conductivity of the sensor, where the electrical resistance per unit length for IM7/PEI tape, ARACON tow, and copper wire are 50 Ω/m, 1.3 Ω/m, and $1.7 \times 10^{-8}/\pi r^2$, respectively.

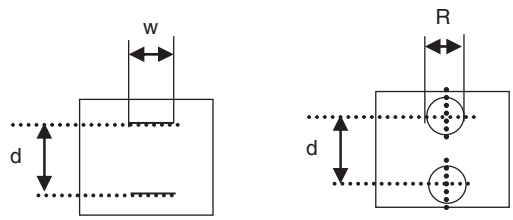

Figure 13. *Schematic cross-section for DCB specimen showing the geometry parameters for a wire sensor type (right side) and a strip sensor type (left side), where R is the wire diameter ($r = R/2$) and w is the width of the strip.*

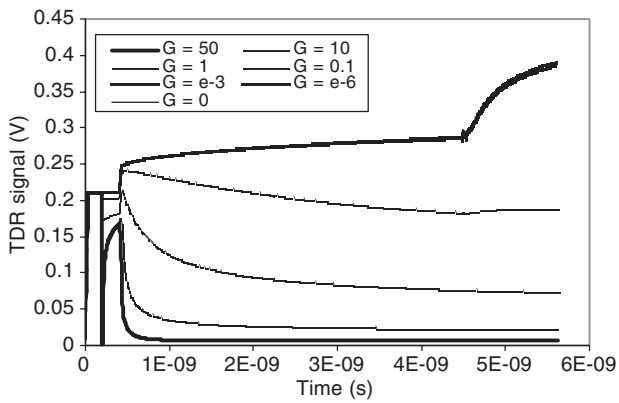

Figure 14. *Effect of substrate conductivity on the TDR sensor response.*

Figure 14 shows the TDR sensor response where the substrate conductivity is varied over several orders of magnitude (G represents the conductivity per unit length of the substrate). The open circuit reflection at the end of the sensor is only seen when conductivities are approximately 10^{-3} or lower. Insulative substrates such as polymers, glass or Kevlar fiber composites, and ceramic matrix composites can be easily evaluated

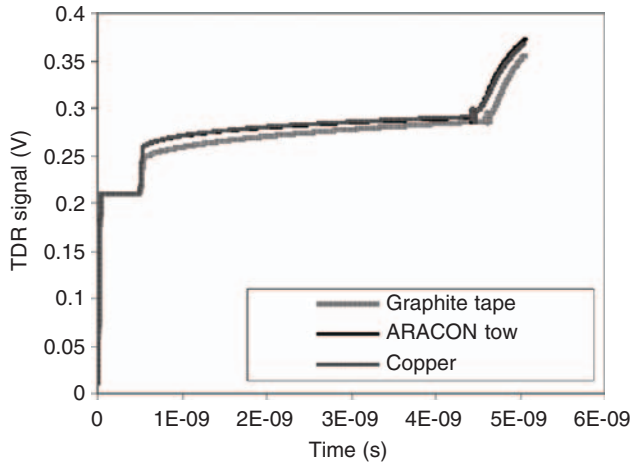

Figure 15. *Effect of sensor conductivity on the TDR sensor response.*

using the TDR sensor. Carbon fiber composites pose a challenge due to the conductivity of the composite material (they have an electrical resistance per unit length in the range of 0.33 Ω/m in the thickness direction [17]) and will be the subject of future work.

DCB Sensor Conductivity

A second parameter of interest is the inherent conductivity of the sensor material. In this study, two conductive sensors were chosen based on carbon fibers and ARACON, for compatibility from a structural aspect with the substrate. Both sensors have lower conductivity than copper, which is a logical choice for a transmission line material. Figure 15 shows a TDR response comparison between copper, ARACON, and carbon fibers, showing no significant difference in the sensor response. Hence, from a cost aspect, standard copper wire can provide excellent TDR sensor performance and can be easily integrated into the specimens during fabrication.

DCB Sensor Geometry

Based on the use of conductive tapes (IM7/PEI) or wires (Aracon tow) for the transmission line, two sensor configurations are of interest. The first configuration uses flat strips (prepreg tape for example) for both the signal and ground plane, separated by a distance d (Figure 13 (left)). The second configuration is similar, except for the use of round conductor (tow bundle or metal wire) for both signal and ground (Figure 13 (right)). In both cases, the signal line geometry (tow diameter or tape width) compared to the ground geometry can play a role in the sensitivity of the sensor response.

Figure 16 compares the TDR sensor response for varying signal line radius (wire or tow) for a fixed ground line radius. There is no significant difference in the TDR sensor response for the various wire geometries. As seen in Figure 17, the spacing between

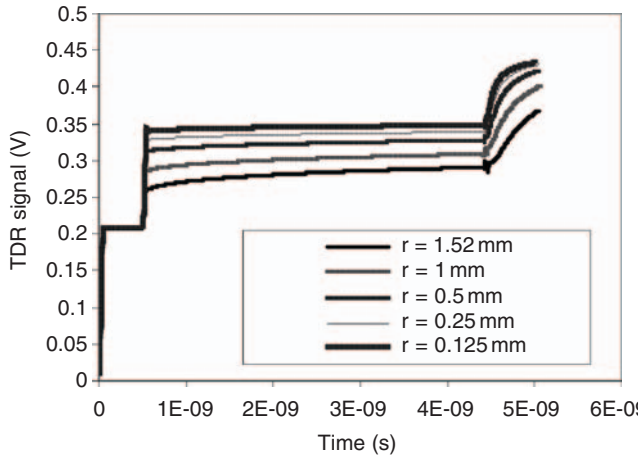

Figure 16. *Effect of signal wire diameter on the TDR sensor response (ground wire diameter fixed at 1.52 mm).*

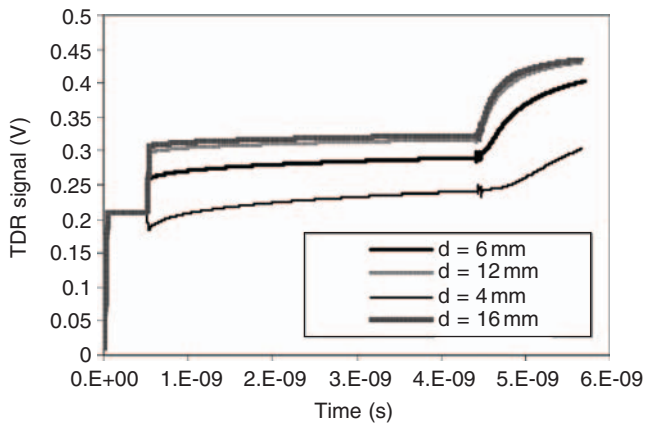

Figure 17. *Effect of the spacing between the signal and the ground paths on the TDR-response.*

the signal and the ground also does not significantly affect the signal, except for changing the effective impedance between the signal and the ground (shifting the signal up or down). The characteristic end reflection is evident in all cases, which is the key metric to be able to detect crack propagation.

In this work, parametric studies on the effect of the geometry parameter (width) of tape or microstrip sensor were not performed. The edge effects of the sensor can dominate the impedance strongly, resulting in a complexity of determination of input parameters (such as L and C). These parameters can be determined as a function of the width of the sensor using finite element method, which is beyond the scope of this study. However, the sensors with cylindrical geometry are sufficient to provide a good TDR signal response for detection of the crack propagation in composites.

CONCLUSIONS

A time-domain reflectometry (TDR) based low-cost and automated solution has been demonstrated for crack detection and propagation measurements during mode 1 DCB testing of composite structures. The TDR technique detects change in geometry or electromagnetic properties along a transmission line that can be embedded in or bonded to a material or a structure. Crack initiation and propagation cause gross changes in these properties and hence are easily detected, with high resolution. The proposed method has the potential to detect the development and propagation of cracks during the test, regardless of temperature, humidity, and other external conditions. It is a fully automated crack sensor with no visual observation required as in current techniques.

Two sensor materials were evaluated to demonstrate flexibility in the sensor material, the first using carbon fiber thermoplastic prepreg tape (IM7/PEI) and the second using ARACON fiber tow (conductive Kevlar) as the transmission line. For all DCB coupons, the sensor geometry used consists of a signal line and a ground line straddling the crack plane of the specimen. For both sensor materials, the crack length (L_C) and fracture toughness (G_{IC}) were measured and compared using the visual method and the TDR system. The TDR method provided excellent correlation with the visual method for crack locations, while providing an order of magnitude improvement in resolution. This enabled more accurate data reduction for the calculation of fracture toughness values in accordance with ASTM D5528.

A P-SPICE based transmission line model was formulated to simulate the TDR sensor and crack propagation in the substrate. Results show a sensitivity of the order of 0.3 mm for specimens with a TDR sensor of a signal-ground spacing of 6 mm, indicating that the signal is being detected near the leading edge of the crack formation. The model was also used to perform parametric studies to evaluate and optimize the sensor. Parametric studies show that the sensor material can be either conductive metal (copper) wire or conductive tow (ARACON), the sensor geometry can be in tape or wire form, no specimen geometry modification is needed and that substrate conductivity can limit applicability of this technique.

The proposed method can be applied to all nonconducting materials – plastics, ceramics, and composites. In the case of electrically conductive systems, especially with carbon fiber reinforcement, the proposed method needs to be modified to account for material conductivity and is a topic of current research. The automation and ease of sensor installation and setup allow the proposed technique to be used in extreme environments, temperature, humidity, corrosive, etc. Demonstrations of the TDR method for hot-wet fracture toughness measurement and low temperatures are in progress.

From overall results, the TDR method has the ability to continuously measure the crack propagation length and crack rate at high resolution and accuracy using low-cost sensors such as copper wire. The entire measurement process can be fully automated to show load–crack growth during the DCB test. The TDR sensors also have enough resolution to detect stick–slip behavior that is characteristic of composite materials. The proposed methodology could also be adapted for mode 2, mode 3 and mixed mode fracture tests, as well as real time crack detection and monitoring in materials and structures. The TDR technique also has significant capabilities in the structural health monitoring field. Since this method does not require visual access, the hard-to-reach zones

in the composite structures can be monitored easily with this technique. The sensor has been successfully used to monitor the manufacture and cure of composite structures and can later be used for health monitoring, providing a cradle-to-grave capability unlike any other system.

NOMENCLATURE

L_C = actual crack length
G_{IC} = interlaminar fracture toughness
G_{ICO} = initiation value of interlaminar fracture toughness
G_{ICP} = propagation value of interlaminar fracture toughness
t_1 = time at which the injection of TDR pulse occurs
t_2 = time at which the reflection of the TDR pulse from far-end termination occurs
t_C = time at which the TDR signal departs from the initial baseline
$L_{opening}$ = total horizontal delamination in the DCB specimen
v = propagation velocity in the sensor of length
L_0 = length of the TDR sensor
L_{CT} = total crack length
α = a statistical threshold limit used to obtain the TDR pulse deviation from the baseline
σ = average standard deviation of the difference between the signal and the baseline, obtained between times t_1 and t_2
A = a constant that depends on the degree of noise in the signal and allows elimination of outliers
$B_i(t)$ = TDR baseline data set
$C_i(t)$ = TDR data during crack propagation
$DC_i(t)$ = TDR difference data set
P = applied load
δ = cross-head displacement
J = compliance factor
n = slope of the plot log J-log(L_{CT})
L = inductance
Z = impedance
C = capacitance
d = distance between the signal line and the ground line
a_0 = initial delamination length
c = DCB specimen length
b = DCB specimen thickness
r = radius of a wire used as a TDR sensor
w = width of a strip or tape used as TDR sensor

ACKNOWLEDGMENTS

This work is partially supported by the National Science Foundation under SBIR Grant No: 0215081.

REFERENCES

1. ASTM D5528-94a, Standard Test Method for Mode I Interlaminar Fracture Toughness of Unidirectional Fiber-Reinforced Polymer Composites, In: *Annual Book of ASTM Standard*, Vol. 08.01.
2. Uhlig, C., Kahle, O., Wieneke, B. and Bauer, M. (2000). Optical Crack Tracing – A New Method for the Automatic Determination of Fracture Toughness for Crack Initiation and Propagation, In: *International Conference and Poster Exhibition MicroMat 2000*, Berlin, pp. 618–629.
3. http://www.lavision.de/products/systems/opticalcracktracer/index.htm (Accessed date: November 23, 2005).
4. http://www.rumul.ch/240_e_fractomat.htm (Accessed date: November 23, 2005).
5. http://www.vishay.com/brands/measurements_group/guide/500/lists/cpglist.htm (Accessed date: November 20, 2005).
6. Time Domain Reflectometry Clearinghouse: http://iti.acns.nwu.edu/clear/tdr (Accessed date: November 20, 2005).
7. Crane, R.M., Gillespie, Jr., J.W., Heider, D., Yarlagadda, S. and Advani, S.G. (2003). Intelligent Processing and Inspection of Composite Materials for Naval Structures, *AMPTIAC Quarterly*, **7**(3): 41–48.
8. High-Performance Composites Magazine, March 2003, pp. 30–31.
9. Hager III, N.E. and Domszy, R.C. (2001). Time-Domain-Reflectometry Cure Monitoring, In: *SAMPE International Symposium*, Long Beach, CA, pp. 2252–2267.
10. NSF SBIR (2003). Nanosecond Pulsed Sensor System for Intrinsic Structural Health and Cure Monitoring.
11. Wadell, B.C. (1991). Transmission-Line Design Handbook, Artech House, Norwood, MA.
12. Applied Wave Research, Inc. www.mwoffice.com/products/txline.html.
13. Yarlagadda, S., Abu Obaid, A., Yoon, M.K., Hager, N. and Domszy, R. (June 7–10, 2004). An Automated Technique for Measuring Crack Propagation during Mode I DCB Testing, *Society of Experimental Mechanics*, X International Congress, Hilton Costa Mesa.
14. Evett, S.R. (2003). Soil Water Measurement by Time Domain Reflectometry, In: Stewart, B.A. and Howell, T.A. (eds), *Encyclopedia of Water Science*, Marcel Dekker, Inc. NewYork, pp. 894–898.
15. P-SPICE Circuit Simulator, Student Version, Download from www.orcad.com (Accessed date: November 23, 2005).
16. Liao, S.Y. (1980). *Microwave Devices and Circuits*, Prentice Hall, Englewood Cliffs, NJ 07632.
17. Rudolf, R., Mitschang, P. and Neitzel, M. (2000). Induction Heating of Continuous Carbon-Fibre-Reinforced Thermoplastic, *Composites: Part A*, **31**: 1191–1202.